Intermetallics 129 (2021) 107050

Contents lists available at ScienceDirect

Intermetallics

journal homepage: http://www.elsevier.com/locate/intermet

Chemical composition dependent local lattice distortions and magnetism in high entropy alloys

Yuan-Yuan Tan [a,1], Ming-Yao Su [a,b,1], Zhou-Can Xie [a,b], Zhong-Jun Chen [c], Yu Gong [c], Li-Rong Zheng [c], Zhan Shi [c], Guang Mo [c], Yong Li [d], Ling-Wei Li [d], Hai-Ying Wang [a,b], Lan-Hong Dai [a,b,e,*]

[a] State Key Laboratory of Nonlinear Mechanics, Institute of Mechanics, Chinese Academy of Sciences, Beijing, 100190, PR China
[b] School of Engineering Science, University of Chinese Academy of Sciences, Beijing, 100049, PR China
[c] Institute of High Energy Physics, Chinese Academy of Sciences & Graduate, University of Chinese Academy of Sciences, Beijing, 100049, PR, China
[d] Institute of Advanced Magnetic Materials, School of Materials and Environmental Engineering, Hangzhou Dianzi University, Hangzhou, 310018, PR China
[e] State Key Laboratory of Explosion Science and Technology, Beijing Institute of Technology, Beijing, 100081, PR China

ARTICLE INFO

Keywords:
Local lattice distortion
Chemical composition
High entropy alloy
Magnetism
XAFS

ABSTRACT

A distinguish feature of high-entropy alloys (HEAs) is well-defined crystalline structure with chemical disorder. While, local lattice distortion is a longstanding issue in HEAs and more challenging than traditional alloys. However, reports on local lattice distortion of HEAs are rarely related to chemical compositions. Here, we use synchrotron radiation facility based XRD and X-ray absorption fine structure (XAFS) to examine averaged lattice distortion and element specified local lattice distortions in CrCoNi medium-entropy alloy (MEA), CrFeCoNi and CrMnFeCoNi HEAs. The results showed that averaged lattice distortions observed from XRD patterns are subtle. The distortion magnitude centred around certain alloying element observed in XAFS spectra keeps in the same order, generally, Ni > Co > Fe > Cr > Mn. The observed positive strains are proposed to counteract negative strains and thus leading to observation of subtle averaged lattice distortion. The XANES results suggested that local electron structure flexibility of element might be one factor that contributes to local lattice distortions. The magnetic measurements indicated a paramagnetic state of all the studied alloys at ambient conditions. This study provides key information on local lattice distortion and its correlations with chemical compositions in HEAs, which is of crucial importance in tailoring properties of advanced HEAs and other multicomponent alloys.

1. Introduction

As a new alloy design strategy, high entropy alloys (HEAs) have been attracting increasing attention since the first inception in 2004 [1,2], numerous HEAs [3–6] have been discovered and Cantor alloy system (such as equiatomic CrCoNi MEA, CrFeCoNi and CrMnFeCoNi HEAs) has been attracting extensive research interests due to their unprecedented properties such as cryogenic-temperature ductility [7], exceptional damage tolerance [8], superior mechanical behavior [9] etc. Generally, the 3*d* metal HEAs present in a single phase with simple face centred cubic (FCC) structure and chemical disorder. Occupation of the same crystallographic sties with atoms of different sizes and lacking of chemical periodicity make the atoms in HEAs displacing from their idealistic lattice positions, subsequently, local lattice distortion is expected and further proposed playing a vital role of importance on mechanical performance [10,11], solid solution strengthening [12,13], phase stability [14–17], and atomic diffusion capacity [18,19], etc. The presence of local lattice distortion is energetically unfavorable [20–22], but it plays a crucial role on mechanical performance of metals. Although, Hume-Rothery rules [23] and Vegard's law [24] are extensively used in binary alloys to evaluate lattice distortions, apparent deviations from Vegard's law in CrCoNi MEA and CrMnFeCoNi HEA have been reported [25]. Hence, local lattice distortion always exists even in traditional alloys. However, the characterization of local lattice distortion becomes more challenging in HEAs because of the complex chemical composition. Characterization methods such as XRD and pair distribution function (PDF) provide averaged lattice distortions of the whole crystal structure, thus, the limitations on resolving local lattice

* Corresponding author. State Key Laboratory of Nonlinear Mechanics, Institute of Mechanics, Chinese Academy of Sciences, Beijing, 100190, PR China.
E-mail address: lhdai@lnm.imech.ac.cn (L.-H. Dai).
[1] The two authors contributed equally to this paper.

https://doi.org/10.1016/j.intermet.2020.107050
Received 2 October 2020; Received in revised form 15 November 2020; Accepted 22 November 2020
Available online 30 November 2020

Table 1
Chemical compositions of CrCoNi MEA, CrFeCoNi HEA and CrMnFeCoNi HEA obtained from the EDS spectra.

Composition / at. %	CrCoNi MEA	CrFeCoNi HEA	CrMnFeCoNi HEA
Cr	35.9	26.9	21.4
Co	32.8	24.5	19.2
Ni	31.3	23.0	17.8
Fe	-	25.6	21.0
Mn	-	-	20.6

distortions around specified chemical compositions in HEAs are obvious. As such, more quantitative studies are endeavored to tackle this issue for enhancing our understanding of structure-property relationships.

As it was firstly proposed by Yeh [27] that lattice structure distortions in CrMnFeCoNi HEA are expected to be severe, however, the experimental results obtained by total scattering [26,28], HRTEM [10] and Extended X-ray absorption fine structure (EXAFS) [29,30] evidenced the absence of serious lattice distortions. Similar contradictory experimental observations have also been reported in CrFeCoNi HEA [28,31]. Furthermore, disagreements on local lattice distortion between simulations and experimental observations have been frequently reported [28,29,32]. Obviously, more further dedicated studies are required. Yet, several parameters or models have been tried from the viewpoints hard sphere model [15], soft sphere assumption [33–35], valence electron concentration [36], and so on [21]. However, to the best of our knowledge, investigations of local lattice distortion correlating to each chemical composition have been reported very limited, although chemical short range order plays as a key factor on structure-property tailoring [37], particularly, in multicomponent alloys [38–40]. Hence, it is of vital importance to decipher associations between local lattice distortions centred around specific chemical composition.

In the present study, we use synchrotron radiation based XRD and EXAFS to interpret averaged lattice distortion and element specified local lattice distortion in CrCoNi MEA, CrFeCoNi and CrMnFeCoNi HEAs. We provide detailed local atomic structure evolutions with chemical complexity increase and calculated the standard deviation of atom pair distance to quantitatively assess local lattice distortions centred around each composition element. To the best of our knowledge, we firstly reported the correlations between local lattice distortion and chemical composition in CrMnFeCoNi system. We further addressed that the origin of local lattice distortion closely relates to local electron structure flexibility. Magnetic properties were characterized to deepen understandings on correlations among physical property, lattice structure, and chemical compositions of CrMnFeCoNi HEAs system.

2. Materials and methods

The most representative FCC structured CrCoNi MEA, CrFeCoNi and CrMnFeCoNi HEAs were produced in near equal atomic composition (Table 1) by arc melting for five times and homogenized at 1473 K for 24 h, air cooling, cold rolling, annealing (1073 K, 1 h) were also conducted to obtain grain size controlled ingots for lattice distortion investigations. Electron backscattering diffraction pattern (EBSD) was collected on JEOL JSM-7900F under 20 kV with a current of 15 nA. The EBSD data collecting step is 1 μm with a total area of 433 × 433 μm^2. Energy-dispersive X-ray spectroscopy (EDS) is collected to characterize chemical compositions.

10 mm × 10 mm × 0.7 mm sized samples were cut from the ingots and polished the surface for the following XAFS and XRD measurements. XAFS data were collected in transmission mode from *K* edges of Cr, Mn, Fe, Co and Ni at 4B9A and 1W2B stations in Beijing Synchrotron Radiation Facility (BSRF). XRD measurements were carried out at 4B9A station using an X-ray wavelength of 1.5406 Å with a scanning step of 0.02° in a two theta range from 30 to 100°.

Magnetic properties of the samples were measured by Vibrating Sample Magnetometer (VSM) affiliating to Dynacool PPMS system from American Quantum Design with a temperature stability better than ± 0.2%, and a magnetism resolution higher than 0.2 mT. Hysteresis loops (M − H curve) were collected at 300 K in a magnetic field of ±5T.

3. Results and discussions

3.1. Microstructure and chemical composition

Table 1 shows the chemical compositions of CrCoNi MEA, CrFeCoNi HEA and CrMnFeCoNi HEA, which are in a near equiatomic ratio as expected. The EBSD inverse pole map (IPF) in Fig. 1 indicates that the three alloys do not have preferred orientations but contain many annealing twins. The average grain sizes of CrCoNi MEA, CrFeCoNi HEA and CrMnFeCoNi HEA were calculated to be 23.4, 22.7 and 20.3 μm.

3.2. Crystalline structure and microstrain

Fig. 2 displays XRD patterns of the as-prepared CrCoNi MEA, CrFeCoNi HEA and CrMnFeCoNi HEA, the three alloys are all in a single phase with well-defined FCC structure. The diffraction peaks in Fig. 2 (a) do not show apparent damping and broadening in CrFeCoNi and CrMnFeCoNi HEAs compared with that of CrCoNi MEA, implying absence of severe local lattice distortions in the alloys, which akin to the previous reports [26,28]. The lattice parameters ***a*** of CrCoNi MEA, CrFeCoNi and CrMnFeCoNi HEAs presented in Fig. 2(b) are 3.509(2) Å, 3.547(2) Å, 3.594(1) Å, which are calculated through Rietveld refinement using High Scoure suite [41], illustrating that the lattice of

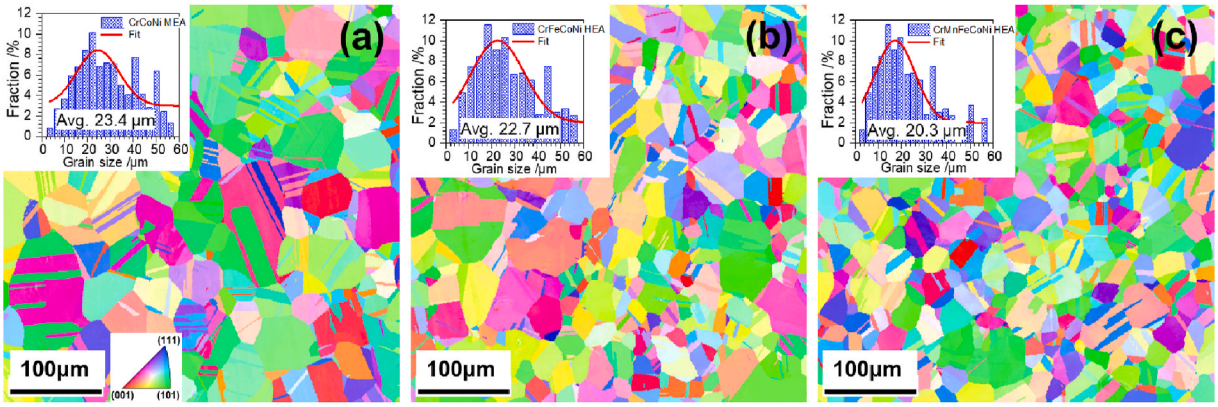

Fig. 1. IPF images and grain size distributions of (a) CrCoNi MEA, (b) CrFeCoNi HEA and (c) CrMnFeCoNi HEA extracted from EBSD data sets.

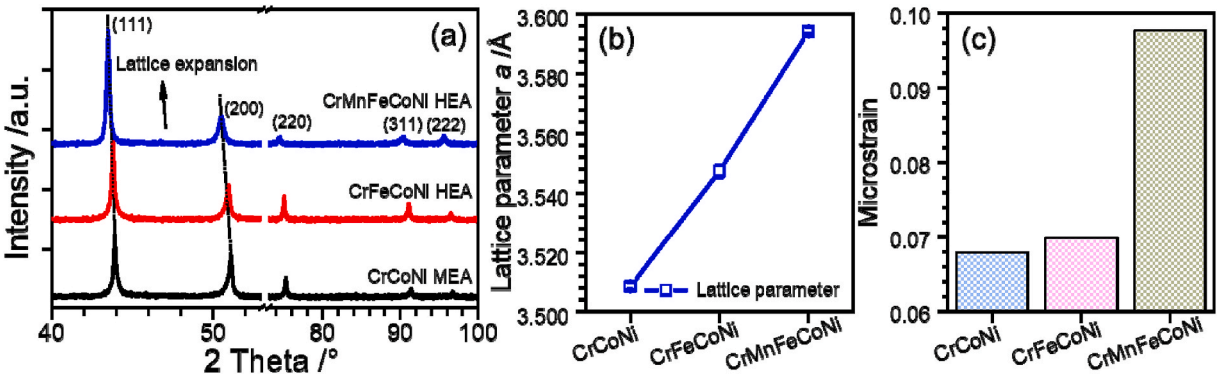

Fig. 2. Crystalline structure and microstrain evolutions in CrMnFeCoNi alloy system. (a) XRD patterns of CrCoNi MEA (bottom), CrFeCoNi (middle) and CrMnFeCoNi (top) HEAs present simple FCC structure. (b) The calculated lattice parameters ***a*** show gradual lattice expansion with chemical complexity increase, and (c) the corresponding growth of microstrain.

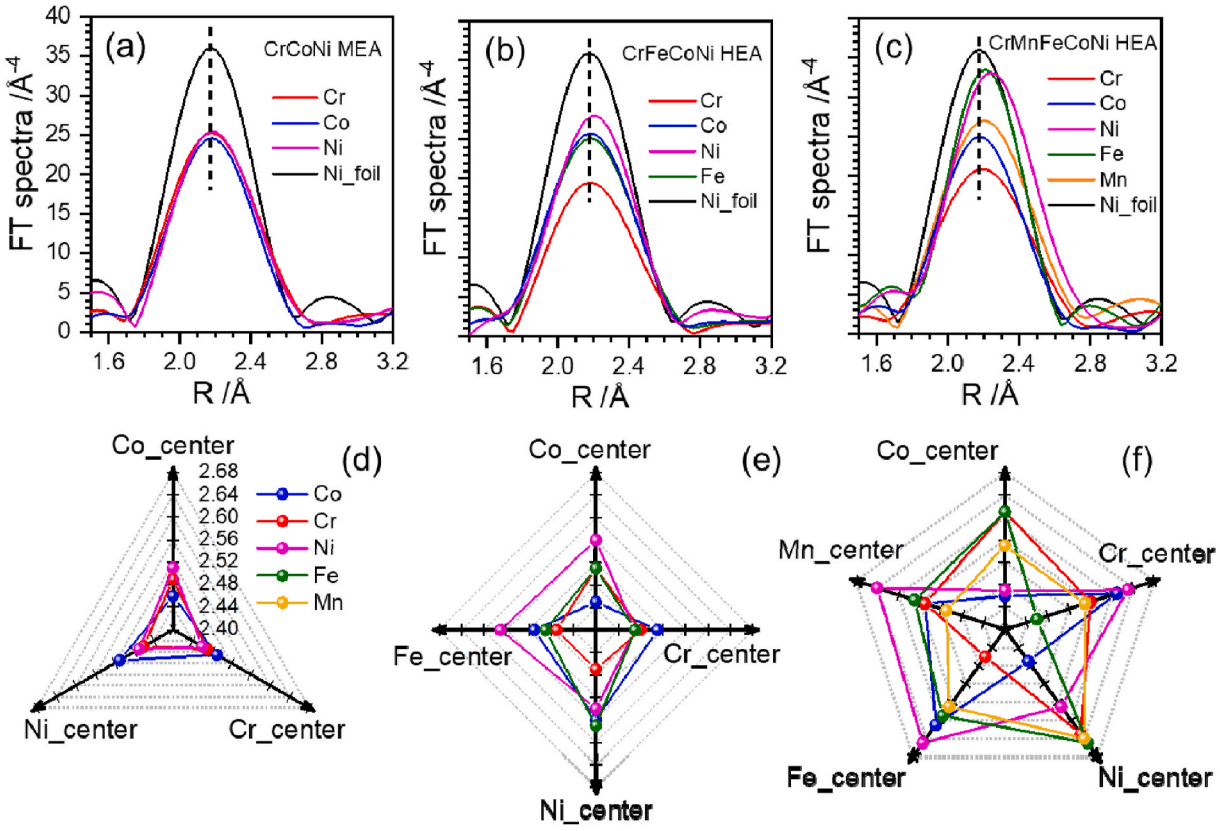

Fig. 3. FT XAFS spectra from *K*-edges of each alloying element in (a) CrCoNi MEA, (b) CrFeCoNi HEA and (c) CrMnFeCoNi HEA, presenting a relatively larger atom pair distance deviation centred around Ni than other alloying composition. The detailed atom pair distances of (d) CrCoNi MEA, (e) CrFeCoNi HEA and (f) CrMnFeCoNi HEA centred around each alloying element.

CrFeCoNi and CrMnFeCoNi HEA have been expanded compared with CrCoNi MEA.

To quantify the averaged lattice distortions, we calculated microstrains by fitting the following equation [42,43]:

$$FWHM^2\cos^2\theta = \left(\frac{\lambda}{d}\right)^2 + \sigma^2\sin^2\theta \quad (1)$$

where FWHM is the full-width at half-maximum of the diffraction peak on the 2θ-scale. The symbols d, λ, σ, and θdenote the grain size, X-ray wavelength, lattice distortion or strain, and diffraction angle, respectively. Fig. 2(c) illustrates that microstrain growth with chemical complexity increase. The results show that increasing chemical complexity would simultaneously induce lattice distortion and averaged lattice expansion, both of them are not significant but actually exist from CrCoNi MEA to CrMnFeCoNi HEA.

It is apparent that adding Mn to CrFeCoNi HEA would cause a lattice parameter increase of 1.33%, while adding Fe to CrCoNi MEA would induce an expansion of 1.08%. At the first glance, we attributed this to a relatively larger effective atomic radius of Mn (1.235 Å) than Fe (1.219 Å) [12]. Supposing the differences between lattice expansions of CrFeCoNi and CrMnFeCoNi HEAs were mainly caused by atomic mismatch, then the lattice of CrMnFeCoNi HEA needs to relax much more than CrFeCoNi HEA to reach a more stable configuration structure after accommodating element with larger atomic radius, which seems to be reasonable. However, both Mn and Fe have smaller effective atomic

radii than Cr (1.269 Å) [12], lattice shrinkage rather than expansion should be observed in CrFeCoNi and CrMnFeCoNi HEAs compared with CrCoNi MEA under the circumstance that all the atoms are hard spheres. Hence, we proposed that the chemical complexity should be another major factor that is mainly responsible for lattice expansions in CrMnFeCoNi system besides atomic radius.

Here comes to another question that how the chemical complexity influences local lattice distortions? The XRD pattern supplied an averaged lattice structure distortion without distinguish local lattice differences among chemical compositions. Then, how about the local lattice distortions centred around specific alloying elements? Therefore, we, in this work, employed XAFS technique to answer this question.

3.3. Local lattice distortions centred around specific alloying element

Local atomic structures centred around each alloying element are carefully examined through analysis of Fourier transformed (FT) XAFS spectrum from the *K*-edges of each element in CrCoNi MEA, CrFeCoNi, and CrMnFeCoNi HEAs using Demeter software package [44]. In CrCoNi MEA (Fig. 3(a)), the averaged atom pair distances centred around Cr, Co and Ni atoms are very close and almost the same with the averaged Ni–Ni atom pair distance in standard pure Ni foil, suggesting subtle lattice expansion and local lattice distortion in CrCoNi MEA compared with standard Ni sample. The averaged atom pair distances centred around Fe, Co and Cr atoms in CrFeCoNi HEA in Fig. 3(b) are slightly larger than averaged Ni–Ni atom pair distance in Ni foil. Noticeably, a larger averaged atom pair distance centred around Ni indicates a greater magnitude of atomic structure distortion around Ni and implies that Ni is under compression in CrFeCoNi HEA, which accords well with simulations [23]. Thus, we remark that the local lattice distortion in CrFeCoNi HEA is highly element dependent, in particular, the local atomic structure around Ni has been distorted to a larger extent than that around Fe, Co, and Cr atoms. This element dependent local lattice distortion becomes more obvious in equiatomic CrMnFeCoNi HEA in Fig. 3(c). The averaged atom pair distance centred around Ni shows the maximum increase, thus confirming that Ni atoms are suffered from compression in CrMnFeCoNi HEA as well as in CrFeCoNi HEA. The averaged atom pair distances centred around Fe and Mn are smaller than Ni but greater than Cr and Co. Evidently, Cr and Co atoms in CrCoFeCoNi HEA are under tension. The evident differences between averaged atom pair distances centred around individual element species indicate a greater magnitude of local lattice distortions in CrMnFeCoNi HEA than CrFeCoNi HEA and CrCoNi MEA, which is in good consistence with the growing microstrains in Fig. 2(c).

Another noticeably feature in Fig. 3(a–c) is the gradual overall elongations of averaged atom pair distances centred around the same element specie from CrCoNi MEA to CrMnFeCoNi HEA, demonstrating lattice expansions with chemical complexity increase. Both of the XAFS and XRD observations confirm the increasing of local lattice distortions with chemical complexity and illustrate highly element dependence of local lattice distortions in CrMnFeCoNi system. Many factors could impact lattice parameters of synthesized materials, such as introducing doping element with different atomic size [45–47], increasing or decreasing sample temperature [48,49], interactions between materials and its interfaces [50], and reducing sample size down to nanometre [51]. For bulk metallic materials, introducing atomic size mismatch are employed often to improve strength of materials through solid solution strengthening [46]. In the binary alloy system, the Vegard's Law described a nearly linear variation of lattice parameter with element content: increasing the content of element with larger atomic size to the base alloy, the lattice parameter of the obtained binary alloy will increase accordingly, and vice versa. As demonstrated by Owen et al. [26], introducing Cr to pure Ni base alloy, the lattice parameter of obtained Ni–Cr alloys increased with increasing Cr content. However, this increasing trend was interrupted when adding a third element Co and a forth element Mn, implying that lattice parameters of HEAs could not be solely determined by atomic size mismatch. Hence, chemical complexity [29] and valance-electron concentration [52] are proposed to illustrate this. As it is commonly recognized that lattice structure would be relaxed through expansion to reach a thermodynamic stabilized configuration structure, we thus proposed that lattice expansion increased with complexity increase in CrMnFeCoNi HEAs might has relaxed local lattice distortions [13,23]. Considering about the reported factors that would cause local lattice distortion in CrMnFeCoNi system, chemical complexity and local electron structure are well discussed on their impacts on local lattice distortion in the following sections.

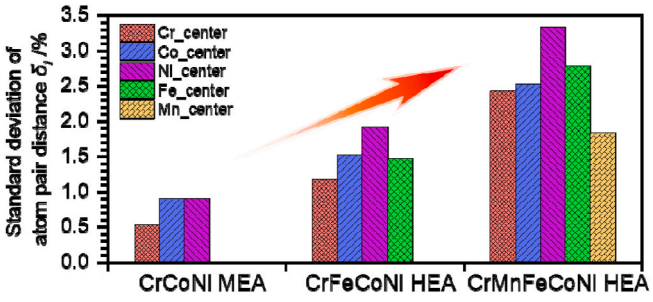

Fig. 4. Calculated standard deviation of atom pair distances δi centred around specific alloying element from the XAFS spectra from *K*-edges of each alloying element.

The specific atom pair distances around each alloying element were obtained by FT-XAFS fitting without phase correction (see fitting details in Supplement Materials) in Fig. 2(d–f). In Fig. 2(d), tiny differences among atom pair distances centred around Cr, Co and Ni are detected in CrCoNi MEA, which consists well with the previous report [53]. However, the atom pair distance differences in CrFeCoNi HEA (Fig. 2(e)) increased apparently, in particular, centred around Ni and Co. The atom pair distances centred around Fe are relatively uniform compared with that around Ni and Co, while, atom pair distances differences around Mn are much smaller. In CrMnFeCoNi HEA, the atom pair distances become more complex, indicating a higher order of local lattice distortion.

To quantitatively assess local lattice distortions centred around specific alloying element, we further calculated standard deviation of atom pair distances centred around specific alloying element from the XAFS fitting results of each alloying element of all the three alloys. The calculation was processed using the following equation:

$$\delta_i = \sqrt{\sum_{i-j}^{n} C_i \left(1 - \frac{r_{i-j}}{\bar{r}}\right)^2} \times 100\% \quad (2)$$

where δ_i is the calculated standard deviation of atom pair distances centred around *i* atom, r_{i-j} is the atom pair distance of *j* atoms centred around *i* atom, $\bar{r}$ is the averaged atom pair distance calculated based on lattice parameter $\boldsymbol{a}$, and $C_i$is the atomic content of *i* atom. A higher δ_i value represents a higher magnitude of local lattice distortion centred around *i* atom. The results in Fig. 4 illustrates that the local lattice distortions centred around Cr, Co and Ni atoms are in the order of Ni > Co > Cr, although XRD pattern verified subtle average lattice distortion in CrCoNi MEA. In CrFeCoNi and CrMnFeCoNi HEAs, the overall local lattice distortions centred around each alloying element have increased gradually, but the magnitude of local lattice distortion centred around specific element keeps in the same order in different alloys, generally, Ni > Co > Fe > Cr > Mn. However, this order is different with either the order of Gold Schmidt radium of the elements or the order of effective atomic radium. As we have mentioned above, the factors that contribute to local lattice distortions in HEA community should consider chemical complexity, more fundamentally, the electron structures, which would be discussed in detail in following section 3.4.

We further calculated the averaged strain around each alloying element using equations (3) and (4) to explore the underlying reasons for the observation of subtle local lattice distortion.

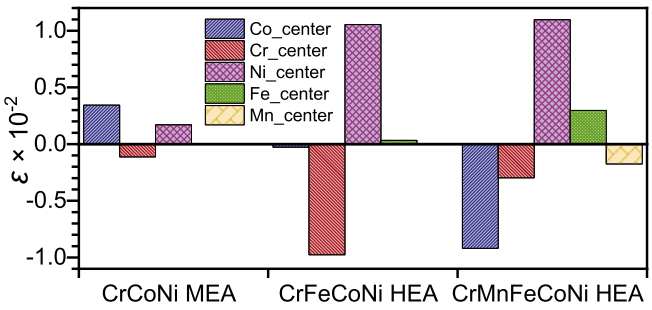

Fig. 5. Averaged strain centred around specific alloying element calculated from the XAFS fitting results.

Table 2
Comparison of lattice distortion between this work and the reported ones.

Sample	ε_{RMS} (%)[a]	ε_{RMS} (%) [54]
CrCoNi	0.33	–
CrFeCoNi	0.72	0.39
CrMnFeCoNi	0.67	3.25
CrFeCoNiPd	–	4.46
$CrFeCoNiAl_{0.375}$	–	4.06

[a] Lattice distortion values calculated from EXAFS in this work.

$$\varepsilon = \frac{\overline{r_i} - \overline{r}}{\overline{r}} \tag{3}$$

$$\overline{r_i} = \sum\nolimits_{i-j}^{n} c_i r_{i-j} \tag{4}$$

where $\overline{r_i}$ is the averaged atom pair distance centred around *i* atom. The results in Fig. 5 showed different positive and negative average strains around each alloying element. In CrCoNi MEA, the absolute value of average positive strains around Co and Ni is slightly larger the negative strain around Cr. In CrFeCoNi HEA, the strains around Co and Fe is very small, however, the absolute value of negative strain around Cr is comparable with that around Ni. Surprisingly, in CrMnFeCoNi HEA, the summary of negative strains around Co, Cr and Mn is almost equal to the positive strains around Ni and Fe. In CrMnFeCoNi alloy system, Ni usually has positive strains and thus undergoes compression, while, Cr has negative strains with tension. Hence, the negative and positive strains presented in Fig. 5 clearly indicate the underlying mechanism for the observation of subtle averaged lattice distortions in HEAs. Averaged lattice distortions do exist in HEAs and increase with chemical complexity in the CrMnFeCoNi alloy system, however, the negative strains counteract positive strains resulting in the observation of subtle lattice distortions. We further evaluated strain fluctuations in the studied alloys using root mean square ε_{RMS} factor and compared with reported lattice distortion values in Table 2. Evidently, the lattice distortions in CrCoNi, CrFeCoNi and CrMnFeCoNi alloys are smaller than those in CrFeCoNiPd and $CrFeCoNiAl_{0.375}$ [54]. Hence, we proposed that atomic size mismatch in multiple components alloys might dominate lattice distortions when the atom radii are quite different, however, other factors, such as chemical complexity and local electron structure variations should be taken into considerations if the atomic size of the components are comparable.

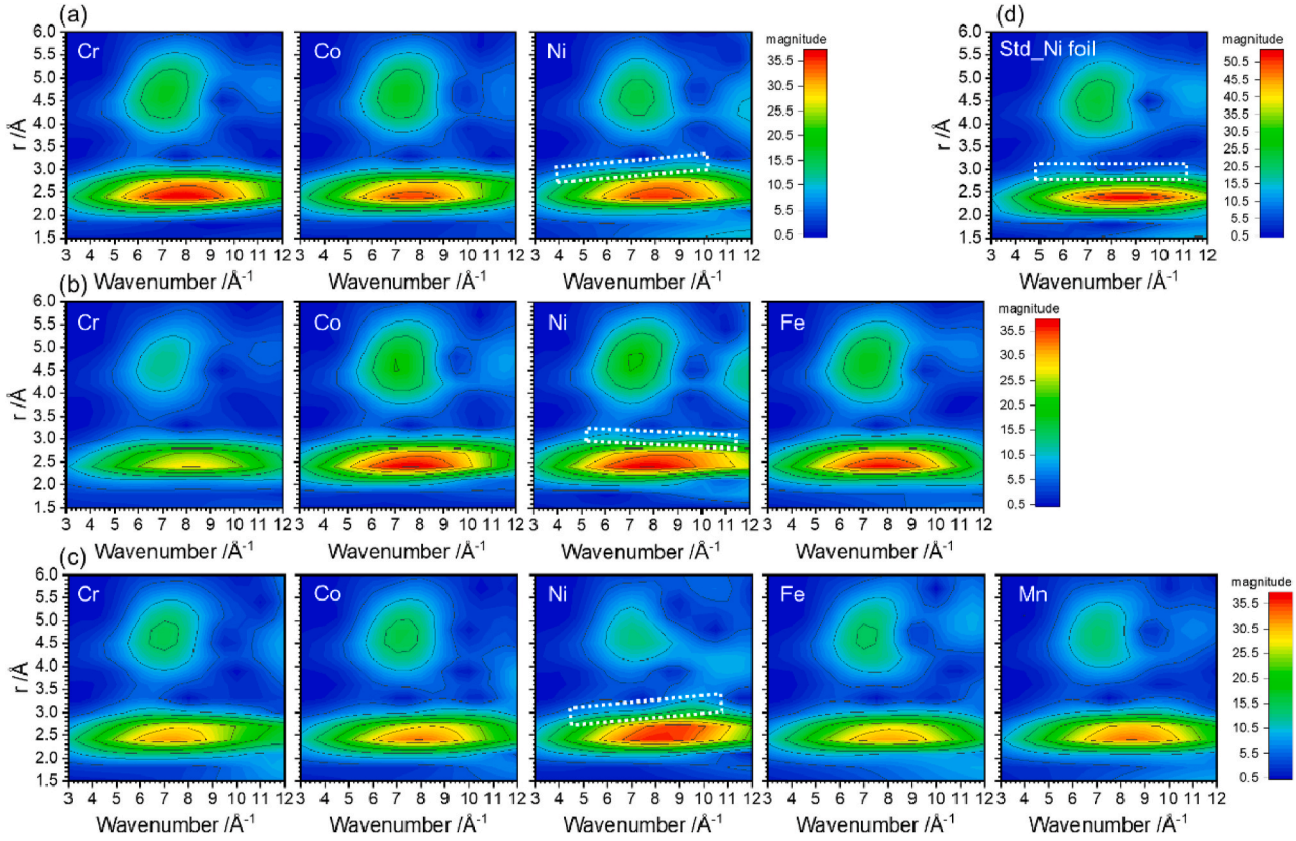

Fig. 6. WT-XAFS spectra from *K*-edges of each component in (a) CrCoNi MEA, (b) CrFeCoNi HEA and (c) CrMnFeCoNi HEA. (d) shows the WT-XAFS of standard Ni foil for an ease of comparison. The peak intensity fluctuations around Ni in CrMnFeCoNi alloy systems are generally more violent than that of Ni foil, indicative of a higher magnitude of local lattice distortion centred around Ni.

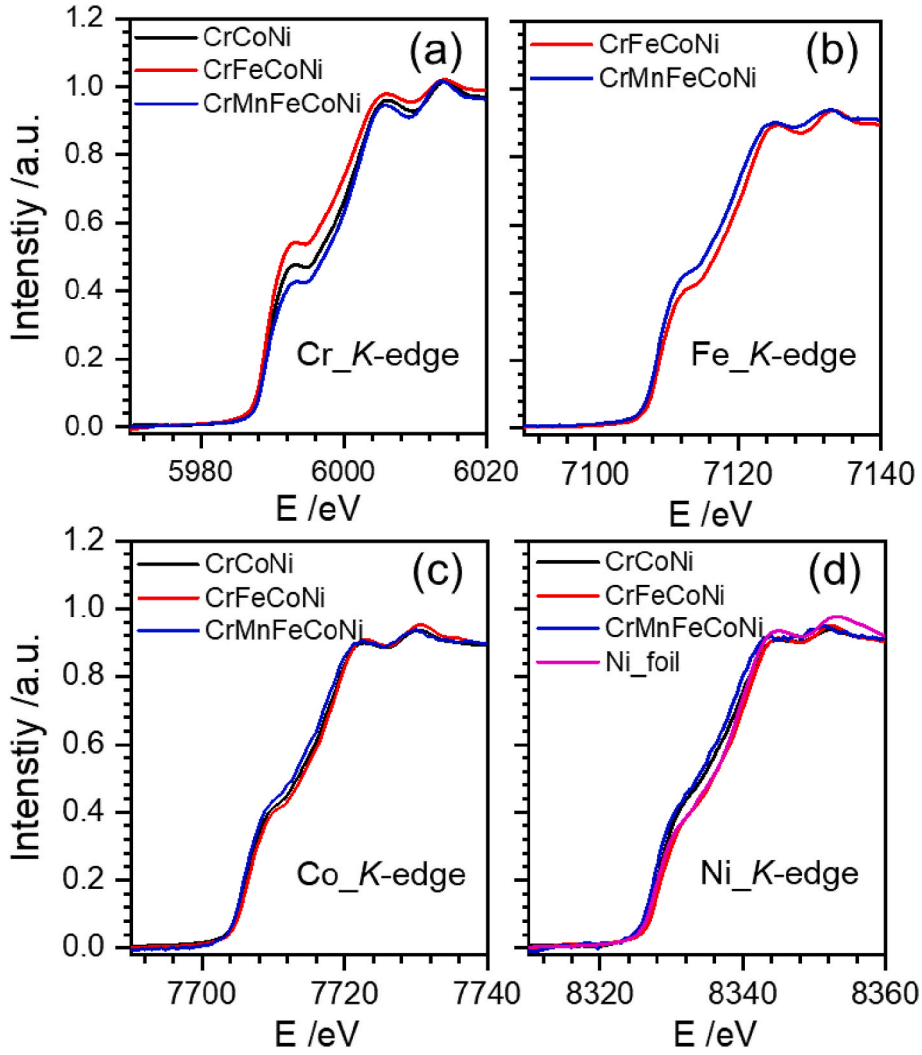

Fig. 7. XANES spectra from *K*-edges of (a) Cr, (b) Fe, (c) Co and (d) Ni in CrCoNi MEA, CrFeCoNi and CrMnFeCoNi HEAs. Differences on electron structure flexibilities of component elements when alloying in multicomponent alloys have been clearly presented.

3.4. Local lattice distortions from WT-XAFS

We further performed wavelet transformation (WT) of the collected XAFS spectra (WT-XAFS) as shown in Fig. 6(a–c) to explore possible atom pair coordination peaks. However, no additional peak intensity was observed besides the main one around 2.3–2.5 Å. Probably, the differences between each favourable atom pair distance are too small to be distinguished, again valid that the local lattice distortion in CrMnFeCoNi system is not severe. Interestingly, we found that the peak intensity of Ni center has more violent fluctuations along *k* axis compared with that of standard Ni foil spectrum (Fig. 6(d)). Considering the standard deviation of atom pair distances centred around Ni in CrCoNi MEA, CrFeCoNi HEA and CrMnFeCoNi HEA, the obvious intensity fluctuations were attributed to a higher magnitude of local lattice distortion centred around Ni than other alloying elements.

3.5. Local electron structure flexibility of alloying elements in HEAs

As it is proposed that electronic structure has significant effects on local lattice distortions in HEAs [36]. However, few experimental data have been reported on addressing this issue. Thus we examined the local electron structure variations of element species from the X-ray absorption near edge structure (XANES) spectra. After background removing, normalized XANES spectra from Cr *K*-edge (Fig. 7(a)) present clear fluctuations when alloying in CrCoNi MEA, CrFeCoNi and CrMnFeCoNi HEAs, while the XANES structures from Ni and Co *K*-edges present much smaller variations in Fig. 7(b–c), indicating that electron structure of Cr varies notably in different alloys but those of Ni and Co are relatively stable. The *d* band of Cr is half full making it very flexible and easier to be affected by its local alloying environment, whereas the *d* band of Ni is nearly full and 80% full for Co, leading to a strong resistance of *d* electron variations during alloying. In contrast, averaged atom pair distances centred around Ni in both CrFeCoNi and CrMnFeCoNi HEAs have the largest deviations from that in standard Ni foil. While the averaged atom pair distances centred around Cr in all the three alloys have slight deviations. The fluctuations around Fe is in between of Cr and Co, Ni in Fig. 7(b).

It seems that Cr acts more like soft sphere during alloying, its high local electronic structure flexibility [55] promotes it adjusting its effective atomic radius to accommodate the lattice structure well and thus inducing little local lattice distortions around Cr. Nevertheless, Ni acts more like hard sphere, it is difficult to tune electronic structures accordingly in line with the lattice structure relaxation and subsequently retaining greater local lattice distortions than Cr. Apparently, the intrinsic electron structure flexibility has significant effects on averaged atom pair distances of individual element species, more generally, local lattice distortions. It is thus reasonable to conclude that local electron structure flexibility of elements differs significantly when alloying in

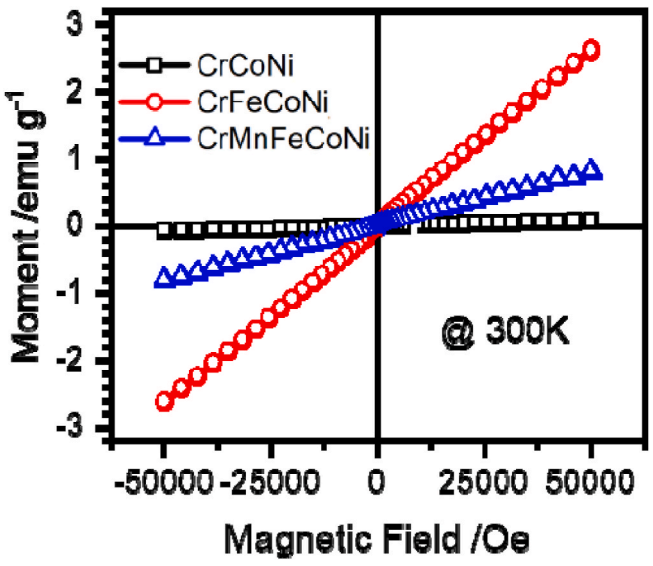

Fig. 8. Magnetization vs. magnetic field (M – H) curves of CrCoNi MEA, CrFeCoNi and CrMnFeCoNi HEAs at 300 K.

different multicomponent alloys. Hence, the local electron structure is proposed as one of the factors that contribute to local lattice distortions.

3.6. Magnetic properties

The calculation results [56–59] demonstrated that lattice structure and chemical composition of HEAs have close correlations with their magnetic properties, therefore, we measured hysteresis loops (M – H curves) of CrCoNi, CrFeCoNi, and CrMnFeCoNi alloys at 300 K to further explore magnetic properties of all the studied alloys. The magnetic moment increased linearly with applied magnetic field in Fig. 8, reaching to 0.07, 2.61, and 0.81 emu/g for CrCoNi, CrFeCoNi, and CrMnFeCoNi, respectively, at 5T under ambient conditions. Clearly, all the studied three alloys are paramagnetic at ambient conditions, agreed well with theoretical calculations from Vitos et al. [56]. Although the magnetic moment values are very small for all the three alloys, increasing trend from CrCoNi to CrFeCoNi alloys was observed, probably, due to high Fe concentrations. However, the magnetism decreased for CrMnFeCoNi compared with CrFeCoNi and very small increase compared with CrCoNi. We thus proposed that the small magnetism of CrCoNi, CrFeCoNi, and CrMnFeCoNi might have little impact on their lattice structures at ambient conditions.

4. Conclusions

In summary, we have demonstrated that averaged lattice distortions and element specified local lattice distortions in CrMnFeCoNi systems will increase with chemical complexity, although the observations are subtle. The XRD patterns verified a subtle averaged lattice distortion and gradual lattice expansion with chemical complexity increase. FT-XAFS presented that local lattice distortions centred around specific alloying element are in the order of Ni > Co > Fe > Cr > Mn, and this order is kept in CrCoNi MEA, CrFeCoNi and CrMnFeCoNi HEAs. Positive strains were observed around Ni, while, negative strains were observed around Cr. The counteract positive and negative strains is proposed as the reason for observation of subtle averaged lattice distortion. Furthermore, WT-XAFS spectra demonstrate more violent peak intensity fluctuations around Ni centres than others, further confirmed the FT-XAFS observations. XANES results proposed that electron structure flexibilities in different alloys might be one major factor that contributes to local lattice distortions. The magnetic measurements indicated a weak paramagnetic state of all the three alloys at ambient conditions.

CRediT authorship contribution statement

Yuan-Yuan Tan: XRD, XAFS experiments, Writing - original draft, Writing - review & editing. **Ming-Yao Su:** Sample preparation, XRD, XAFS experiments. **Zhou-Can Xie:** XRD, XAFS experiments. **Zhong-Jun Chen:** Experiment setup preparations, and XRD, XAFS data collection. **Yu Gong:** Experiment setup preparations, and XRD, XAFS data collection. **Li-Rong Zheng:** Experiment setup preparations, and XRD, XAFS data collection. **Zhan Shi:** Experiment setup preparations, and XRD, XAFS data collection. **Guang Mo:** Experiment setup preparations, and XRD, XAFS data collection. **Yong Li:** Magnetism measurement. **Ling-Wei Li:** Magnetism measurement. **Hai-Ying Wang:** Writing - review & editing, Review, editing, and funding. **Lan-Hong Dai:** Supervision, Writing - review & editing, Funding acquisition.

Declaration of competing interest

The authors declare that they have no known competing financial interests or personal relationships that could have appeared to influence the work reported in this paper.

Acknowledgments

We sincerely thank Prof. Minqiang Jiang, Mr. Gan Ding and Mr. Cheng Yang for their help and kind discussions on the magnetic measurements. This work is supported by the National Key Research and Development Program of China (No. 2017YFB0702003), the NSFC (Nos. 12002341, 11790292, 11672316), the NSFC Basic Science Center Program for "Multiscale Problems in Nonlinear Mechanics" (No.11988102), the Strategic Priority Research Program (Nos. XDB22040302, XDB22040303), the Key Research Program of Frontier Sciences (Grant No. QYZDJSSW-JSC011), Science Challenge Project (No. TZ2016001).

Appendix A. Supplementary data

Supplementary data to this article can be found online at https://doi.org/10.1016/j.intermet.2020.107050.

References

[1] J.W. Yeh, S.K. Chen, S.J. Lin, J.Y. Gan, T.S. Chin, T.T. Shun, C.H. Tsau, S.Y. Chang, Adv. Eng. Mater. 6 (2004) 299–303.
[2] B. Cantor, I.T.H. Chang, P. Knight, A.J.B. Vincent, Mater. Sci. Eng. A 375–377 (2004) 213–218.
[3] J.P. Liu, J.X. Chen, T.W. Liu, C. Li, Y. Chen, L.H. Dai, Scripta Mater. 181 (2020) 19–24.
[4] T. Yang, Y.L. Zhao, Y. Tong, Z.B. Jiao, J. Wei, J.X. Cai, X.D. Han, D. Chen, A. Hu, J. J. Kai, K. Lu, Y. Liu, C.T. Liu, Science 362 (2018) 933–937.
[5] Y. Lu, Y. Dong, H. Jiang, Z. Wang, Z. Cao, S. Guo, T. Wang, T. Li, P.K. Liaw, Scripta Mater. 187 (2020) 202–209.
[6] X.F. Liu, Z.L. Tian, X.F. Zhang, H.H. Chen, T.W. Liu, Y. Chen, Y.J. Wang, L.H. Dai, Acta Mater. 186 (2020) 257–266.
[7] B. Gludovatz, A. Hohenwarter, D. Catoor, E.H. Chang, E.P. George, R.O. Ritchie, Science 345 (2014) 1153–1158.
[8] Z. Li, K.G. Pradeep, Y. Deng, D. Raabe, C.C. Tasan, Nature 534 (2016) 227–230.
[9] E.P. George, W.A. Curtin, C.C. Tasan, Acta Mater. 188 (2020) 435–474.
[10] Q. Ding, Y. Zhang, X. Chen, X. Fu, D. Chen, S. Chen, L. Gu, F. Wei, H. Bei, Y. Gao, M. Wen, J. Li, Z. Zhang, T. Zhu, R.O. Ritchie, Q. Yu, Nature 574 (2019) 223–227.
[11] Z.F. Lei, X.J. Liu, Y. Wu, H. Wang, S.H. Jiang, S.D. Wang, X.D. Hui, Y.D. Wu, B. Gault, P. Knotis, D. Raabe, L. Gu, Q.H. Zhang, H.W. Chen, H.T. Wang, J.B. Liu, K. An, Q.S. Zeng, T.G. Nieh, Z. Lu, Nature 563 (2018) 546–550.
[12] N.L. Okamoto, K. Yuge, K. Tanaka, H. Inui, E.P. George, AIP Adv. 6 (2016) 125008.
[13] L.R. Owen, N.G. Jones, Scripta Mater. 187 (2020) 428–433.
[14] J.Y. He, H. Wang, Y. Wu, X.J. Liu, H.H. Mao, T.G. Nieh, Z.P. Lu, Intermetallics 79 (2016) 41–52.
[15] Y. Zhang, Y.J. Zhou, J.P. Lin, G.L. Chen, P.K. Liaw, Adv. Eng. Mater. 10 (2008) 534–538.
[16] Y.Y. Zhao, H.W. Chen, Z.P. Lu, T.G. Nieh, Acta Mater. 147 (2018) 184–194.
[17] L. Lin, X. Xian, Z. Zhong, C. Chen, Z. Zhu, Y. Wu, Peter K. Liaw, Intermetallics 120 (2020) 106744.
[18] A. Durand, L. Peng, G. Laplanche, J.R. Morris, E.P. George, G. Eggeler, Intermetallics 122 (2020) 106789.
[19] K.Y. Tsai, M.H. Tsai, J.W. Yeh, Acta Mater. 61 (2013) 4887–4897.
[20] L.R. Owen, N.G. Jones, J. Mater. Res. 33 (2018) 2954–2969.

[21] Z. Wang, W. Qiu, Y. Yang, C.T. Liu, Intermetallics 64 (2015) 63–69.
[22] I. Toda-Caraballo, P.E.J. Rivera-Díaz-Del-Castillo, Intermetallics 71 (2016) 76–87.
[23] T. Egami, M. Ojha, O. Khorgolkhuu, D.M. Nicholson, G.M. Stocks, JOM (J. Occup. Med.) 67 (2015) 2345–2349.
[24] E.K.M. Hume-Rothery, G.W. Mabbott, Philos Trans Math Phys Eng Sci 233 (1934) 1–97.
[25] E. Zen, (1956) 5–6.
[26] L.R. Owen, E.J. Pickering, H.Y. Playford, H.J. Stone, M.G. Tucker, N.G. Jones, Acta Mater. 122 (2017) 11–18.
[27] J.W. Yeh, Ann. Chim. – Sci. Des Mater. 31 (2006) 633–648.
[28] Y. Tong, K. Jin, H. Bei, J.Y.P. Ko, D.C. Pagan, Y. Zhang, F.X. Zhang, Mater. Des. 155 (2018) 1–7.
[29] F. Zhang, Y. Tong, K. Jin, H. Bei, W.J. Weber, A. Huq, A. Lanzirotti, M. Newville, D. C. Pagan, J.Y.P. Ko, Y. Zhang, Mater. Res. Lett. 6 (2018) 450–455.
[30] H.S. Oh, D. Ma, G.P. Leyson, B. Grabowski, E.S. Park, F. Kormann, D. Raabe, Entropy 18 (2016) 1–9.
[31] F.H. Cao, Y.J. Wang, L.H. Dai, Acta Mater. 194 (2020) 283–294.
[32] Y.H. Zhang, Y. Zhuang, A. Hu, J.J. Kai, C.T. Liu, Scripta Mater. 130 (2017) 96–99.
[33] Y.F. Ye, C.T. Liu, Y. Yang, Acta Mater. 94 (2015) 152–161.
[34] Y.F. Ye, Y.H. Zhang, Q.F. He, Y. Zhuang, S. Wang, S.Q. Shi, A. Hu, J. Fan, Y. Yang, Acta Mater. 150 (2018) 182–194.
[35] Q. He, Y. Yang, Front. Mater. 5 (2018) 1–8.
[36] S. Guo, C. Ng, J. Lu, C.T. Liu, J. Appl. Phys. 109 (2011).
[37] W. Yang, I.J. Beyerlein, Q. Jin, H. Ge, T. Xiong, L. Yang, J. Pang, Y. Zhou, X. Shao, B. Zhang, S. Zheng, X. Ma, Scripta Mater. 166 (2019) 73–77.
[38] R. Zhang, S. Zhao, J. Ding, Y. Chong, T. Jia, C. Ophus, M. Asta, R.O. Ritchie, A. M. Minor, Nature 581 (2020) 283–287.
[39] Z. Lei, X. Liu, Y. Wu, H. Wang, S. Jiang, S. Wang, X. Hui, Y. Wu, B. Gault, P. Kontis, D. Raabe, L. Gu, Q. Zhang, H. Chen, H. Wang, J. Liu, K. An, Q. Zeng, T.G. Nieh, Z. Lu, Nature 563 (2018) 546–550.
[40] Y.C. Yang, C. Liu, C.Y. Lin, Z. Xia, Scripta Mater. 178 (2020) 181–186.
[41] T. Degen, M. Sadki, E. Bron, U. König, G. Nénert, Powder Diffr. 29 (2014) S13–S18.
[42] K. Zhang, S. Peng, N. Li, X. Liu, M. Zhang, Y.D. Wu, Y. Yang, E. Greenberg, V. B. Prakapenka, X. Hui, Y. Wang, W. Yang, Appl. Phys. Lett. 116 (2020), 031901.
[43] X. Yan, D. Tan, X. Ren, W. Yang, D. He, H.K. Mao, Appl. Phys. Lett. 106 (2015) 171902.
[44] B. Ravel, M. Newville, J. Synchrotron Radiat. 12 (2005) 537–541.
[45] R.K. Nutor, Q. Cao, X. Wang, D. Zhang, Y. Fang, Y. Zhang, J.Z. Jiang, Adv. Eng. Mater. (2020) 1–36, 2000466.
[46] C. Lee, Y. Chou, G. Kim, M.C. Gao, K. An, C. Zhang, W. Chen, J.D. Poplawsky, G. Song, Y. Ren, P.K. Liaw, Y.-C. Chou, Adv. Eng. Mater. (2020) 1–9, 2004029.
[47] S. Kobayashi, Y. Ikuhara, T. Mizoguchi, Phys. Rev. B 98 (2018) 134114.
[48] E.W. Huang, H.S. Chou, K.N. Tu, W.S. Hung, T.N. Lam, C.W. Tsai, C.Y. Chiang, B. H. Lin, A.C. Yeh, S.H. Chang, Y.J. Chang, J.J. Yang, X.Y. Li, C.S. Ku, K. An, Y. W. Chang, Y.L. Jao, Sci. Rep. 9 (2019) 1–10.
[49] S. Huang, Á. Vida, W. Li, D. Molnár, S. Kyun Kwon, E. Holmström, B. Varga, L. Károly Varga, L. Vitos, Appl. Phys. Lett. 110 (2017).
[50] C. Chen, J. Avila, H. Arezki, V.L. Nguyen, J. Shen, M. Mucha-Kruczyński, F. Yao, M. Boutchich, Y. Chen, Y.H.M.C. Lee, Nat. Mater. 17 (2018) 450–455.
[51] Z. Wei, T. Xia, J. Ma, W. Feng, J. Dai, Q. Wang, P. Yan, Mater. Char. 58 (2007) 1019–1024.
[52] W. Zhang, P.K. Liaw, Y. Zhang, Sci. CHINA Mater. 61 (2018) 2–22.
[53] F.X. Zhang, S. Zhao, K. Jin, H. Xue, G. Velisa, H. Bei, R. Huang, J.Y.P. Ko, D. C. Pagan, J.C. Neuefeind, W.J. Weber, Y. Zhang, Phys. Rev. Lett. 118 (2017) 1–6.
[54] Y.F. Ye, Q. Wang, J. Lu, C.T. Liu, Y. Yang, Mater. Today 19 (2016).
[55] S. Zhao, T. Egami, G.M. Stocks, Y. Zhang, Phys. Rev. Mater. 2 (2018) 13602.
[56] S. Huang, E. Holmström, O. Eriksson, L. Vitos, Intermetallics 95 (2018) 80–84.
[57] Z. Dong, L. Vitos, Scripta Mater. 171 (2019) 78–82.
[58] Z. Dong, S. Schönecker, W. Li, D. Chen, L. Vitos, Sci. Rep. 8 (2018) 4–10.
[59] D. Kim, L. Vitos, Sci. Rep. 6 (2016) 1–8.